Journal of ELECTRONIC MATERIALS, Vol. 48, No. 7, 2019
https://doi.org/10.1007/s11664-019-07209-3

Two-Step Preparation of ZnO/ZnSe Heterostructure with Remarkable Photocatalytic Activity by Ultrasonic and Hydrothermal Approach

FEN QIAO,[1,4,5] QICHAO LIANG,[1] XIAOYA HOU,[2] JIAN YANG,[1] and QIAN XU[3]

1.—School of Energy and Power Engineering, Jiangsu University, Zhenjiang 212013, People's Republic of China. 2.—School of Mechanical Engineering, Jiangnan University, Wuxi, Jiang Su 214122, People's Republic of China. 3.—Institute for Energy Research, Jiangsu University, 301 Xuefu Road, Zhenjiang 212013, People's Republic of China. 4.—e-mail: fqiao@ujs.edu.cn. 5.—e-mail: ujsfqiao@163.com

In order to improve the light absorption capacity of ZnO and reduce the charge recombination, the heterostructure of ZnO/ZnSe was prepared by a simple synthetic route. The heterostructure was composed of spherical ZnSe growing on ZnO rod, in which the ZnO rods were synthesized by an ultrasonic method. The concentration of ammonia in the reaction solution was the key factor to determine the nucleation and growth rate of ZnO/ZnSe heterostructure. In addition, the relationship between structure and photocatalytic activity was studied. Compared with bare ZnO rods and spherical ZnSe, as-prepared ZnO/ZnSe heterostructure exhibited excellent photocatalytic activity for the degradation of methyl orange dye, which was attributed to the effective charge transport performance generated by the coupling of ZnO and ZnSe.

Key words: Semiconductor, photocatalytic activity, heterostructure, charge transport

INTRODUCTION

As one of the most promising semiconductor materials in photocatalysis, ZnO has received remarkable attention because of its remarkable chemical and physical properties, especially its non-toxicity and high excitation binding energy.[1–9] However, the photocatalytic application of ZnO has been hindered by serious electron–hole recombination, low visible light utilization and easy aggregation.[10–12] Therefore, to increase the absorption range of light and reduce charge recombination, much efforts have been made to expand the range of light response and suppress charge recombination. Combining ZnO with other narrow-band gap semiconductors can effectively extend its optical response range, such as ZnO/CdS,[13–15] ZnO/Ag,[16–18] ZnO/carbon materials.[19–23] ZnSe is an attractive photocatalyst for converting solar energy into chemical energy and can be achieved through a simple and inexpensive hydrothermal process. The combination of ZnO and ZnSe is expected to be an ideal system for achieving enhanced charge separation. Many studies have focused on the heterostructure of ZnO/ZnSe, but these heterostructures have high cost and complex preparation process.

In this work, we fabricated ZnO/ZnSe heterostructure by combining ultrasonic and hydrothermal methods, in which spherical ZnSe particles grew on ZnO rods. By adjusting the concentration of ammonia in the reaction solution, the rod-like ZnO/ZnSe heterostructures were formed. Compared with ZnO and ZnSe, ZnO/ZnSe heterostructure showed enhanced visible light absorption and photocatalytic activity through its type-II band alignment, which resulted in efficient charge separation and larger active surface. This approach does not require any membrane or

(Received July 30, 2018; accepted April 6, 2019; published online April 24, 2019)

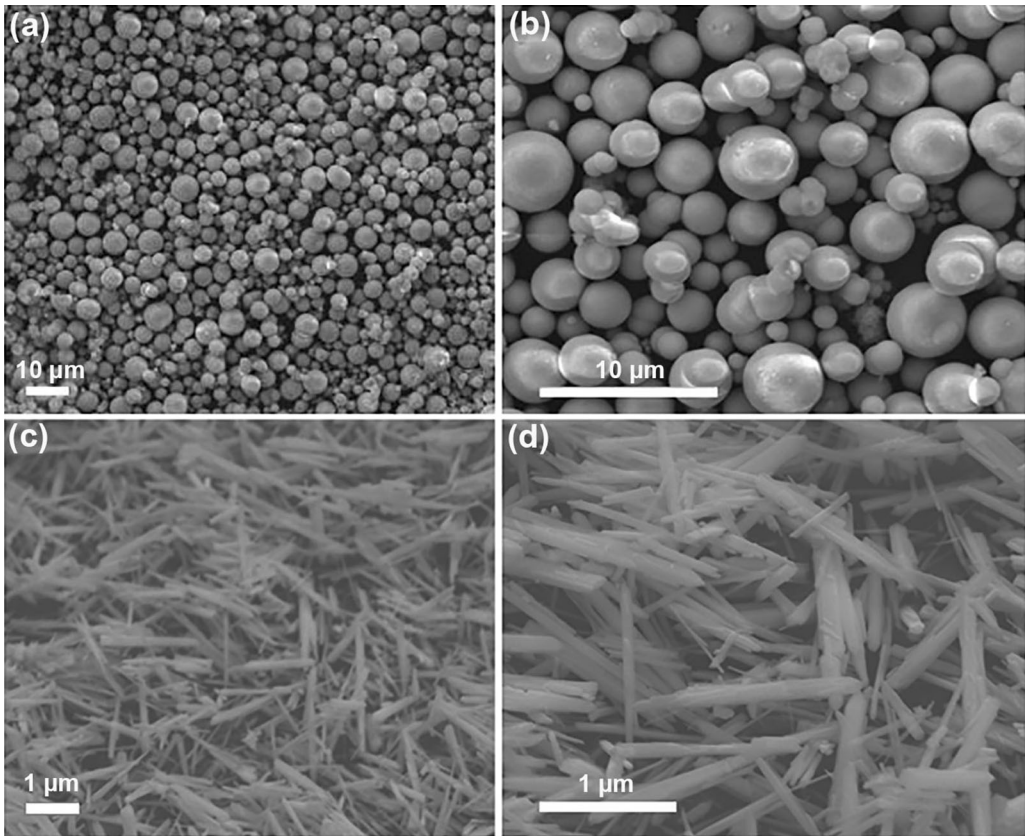

Fig. 1. Low-and high-magnification FESEM images of (a, b) bare spherical ZnSe and (c, d) ZnO rods.

surfactant to generate anisotropic structures to control their orientation. Therefore, this method of preparing a ZnO/ZnSe heterostructure is more environmentally friendly, convenient and inexpensive.

EXPERIMENTAL SECTION

Preparation of ZnO Rods

All chemicals (analytical grade) were purchased from Chinese National Medicine Group and used without purification. ZnO rods were synthesized by ultrasonic method, a mixed solution of zinc acetate (0.035 M), sodium hydroxide (0.45 M) in deionized water (40 mL) was dissolved and then kept in an ultrasonic instrument for 6 h. Finally, the sample was rinsed with deionized water and dried at 80°C for 1 h.

Preparation of Spherical ZnSe

$Zn(NO_3)_2{\cdot}6H_2O$ (0.1 M), Na_2SeO_3 (0.1 M) and NaOH (1 mol/L,20 mL) were added to deionized water (10 mL). The mixed solution was ultrasonically treated until completely dissolved; Subsequently, 10 ml of hydrazine (85%) was added dropwise during vigorous stirring, and transferred the solution into an autoclave and heated at 180°C for 4 h. The sample was washed twice with ethanol and deionized water, and then heated it at 60°C for 8 h.

ZnO/ZnSe Heterostructure

ZnO/ZnSe heterostructure was synthesized by hydrothermal method, in which the as-prepared ZnO rods was chosen as the source. Typically, a mixed solution of ammonia (12.5%, 40 mL), ZnO rods powder (0.025 M), Selenium powder (0.013 M) and $NaBH_4$ (0.007 M) were prepared under stirring and heated at 70°C for 0.5 h. The above solution was put into an autoclave and heated at 90°C for 8 h. The deposit obtained, namely ZnO/ZnSe heterostructure sample, was washed twice with ethanol and deionized water, and dried at 60°C for 8 h for further characterization.

Characterization

The morphology and crystallinity of samples were checked by field emission scanning electron microscope (FESEM, 7800F) and x-ray diffraction (XRD, Bruker Advanced D8), respectively. The photocatalytic performance was measured by photodegradation of methyl orange solution (30 μM, 50 mL) under a 250 W Xe lamp illumination. In general, photocatalyst (50 mg) was dispersed in dye and stirred for 30 min using an ultrasonic instrument. During the whole process of irradiation, stirring

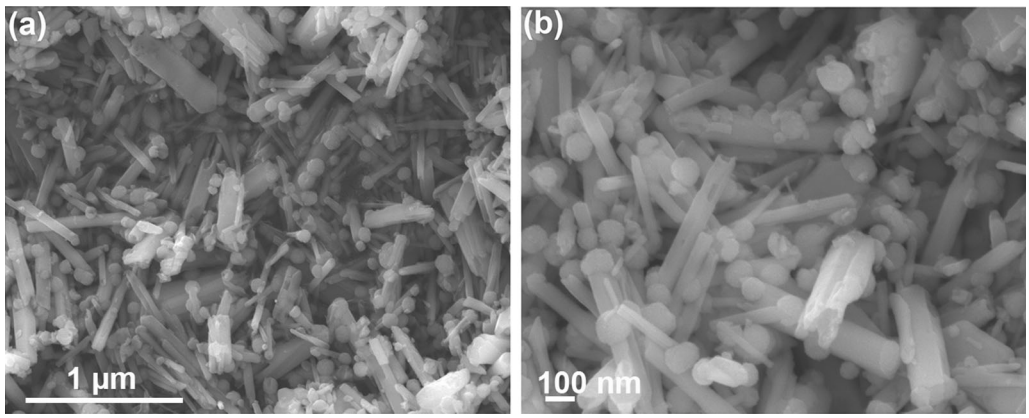

Fig. 2. (a) Low-and (b) high-magnification SEM images of ZnO/ZnSe heterostructures.

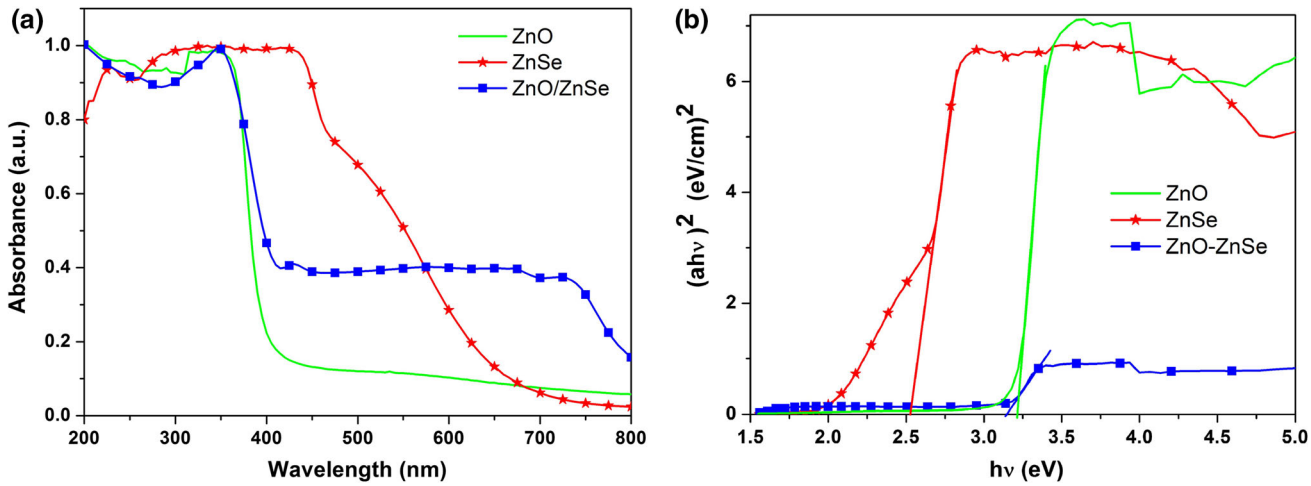

Fig. 3. (a) Absorption spectra and (b) Tauc plots of ZnO rod, ZnSe microsphere and ZnO/ZnSe heterostructure.

was kept to maintain the photocatalyst evenly dispersed. The concentration of methyl orange was monitored by UV–Vis spectrophotometer at a series of time intervals.

RESULTS AND DISCUSSION

The morphology of spherical ZnSe and ZnO rods was characterized by FE-SEM. As shown in Fig. 1a, numerous spherical ZnSe microstructures were formed. Notable, high-magnification images showed the formation of spherical ZnSe particles with irregular contours and they all showed similar morphology (Fig. 1b). The specific surface area provided a large contact areas and improved the photocatalytic efficiency when coupled with the ZnO rods.

Figure 1c shows that SEM image of numerous ZnO rods grown from ultrasonic way. Careful examination revealed the formation of a large number of ZnO with rod structures, and no other structures were observed (Fig. 1d), indicating that ZnO rod was obtained through spontaneous nucleation with high crystal integrity.

Figure 2a shows ZnO/ZnSe obtained from the reaction of the ammonia (12.5%), ZnO rods (0.025 M), Selenium powder (0.013 M) and $NaBH_4$ (0.007 M) solution at 90°C for 8 h. As shown in Figs. 2a and S1a, the rod-like ZnO/ZnSe heterostructure were formed and covered a large area. A closer SEM observation showed that the spherical shape of ZnSe particles grew on ZnO rods (Figs. 2b and S1b). Most ZnSe microspheres were distributed on ZnO rods and almost every ZnO rod was covered by a spherical ZnSe particle, indicating that they weren't formed by random nucleation.

In this reaction process, $NaBH_4$ and ammonia were used as reducing agent and alkaline environment supplier, respectively. With the increase of OH^-, more $Zn(OH)_4^{2-}$ would be generated and further reacted with Se^{2-} to form ZnO/ZnSe heterostructurs.[5–9] The chemical equations involved in the reaction process were as follows:

$$ZnO + H_2O + 2OH^- \rightarrow Zn(OH)_4^{2-} \quad (1)$$

$$Se + 2NaBH_4 \rightarrow Na_2Se + B_2H_6 + H_2 \quad (2)$$

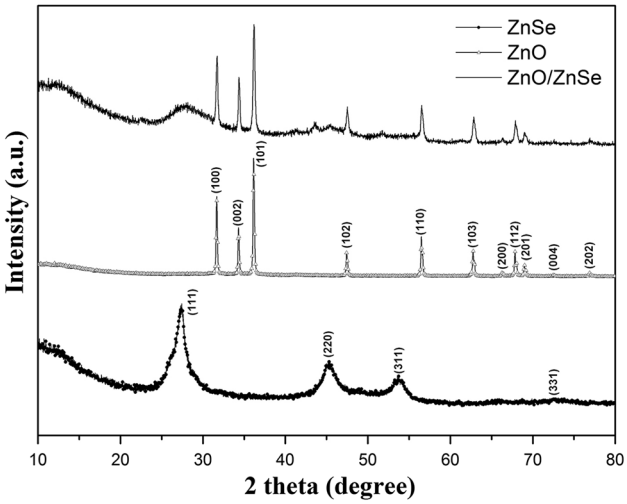

Fig. 4. XRD patterns of the as-prepared ZnO rods (triangle), ZnSe (circle) and ZnO/ZnSe heterostructure (solid line).

$$3Se + 6OH^- \rightarrow 2Se^{2-} + SeO_3^{2-} + 3H_2O \quad (3)$$

$$Se^{2-} + Zn(OH)_4^{2-} \rightarrow ZnSe + 4OH^- \quad (4)$$

The absorption spectra indicated that wide-band gap ZnO had strong ultraviolet absorption, but could only absorb a small amount of visible light (Fig. 3a). ZnSe microspheres had more abroad absorption in visible light region, while ZnO/ZnSe heterostructure had strong absorption in both ultraviolet and visible light range, indicating it might generate more photoelectronic charge to promote photocatalytic degradation of organic dyes. According to the solid UV–visible absorption spectra and Tauc formula, the bandgap of bare ZnO rods, ZnSe microspheres and ZnO/ZnSe heterostructures was calculated as 3.21 eV, 2.52 eV, close to the relevant theoretical value of 3.34 eV and 2.67 eV, respectively. The bandgap of ZnO/ZnSe sample with heterostructure was 3.15 eV, which was narrower than that of bare ZnO.

As shown in Fig. 4, all XRD patterns of ZnO could be indexed as wurtzite structure (JCPDS No. 36-1451) with stronger and narrower characteristic peak strength. The spectral width indicated that the sample had high purity. Diffraction peaks at 27.3°(111), 45.3°(220) and 53.6°(311) made it clear that there were ZnSe cubic phase (JCPDS No. 37-1463). In addition, the sharp diffraction peaks indicated that as-prepared ZnO/ZnSe had good crystalline quality. All the diffraction peaks of ZnO remained in the XRD diagram of ZnO/ZnSe, which confirmed the wurtzite structures nature of ZnO and still existed after the formation of ZnSe. As shown in the XRD patterns (Fig. 4), the presence of ZnO in the composite did not change the cubic phase of ZnSe structure. The successful integration of ZnO and ZnSe could improve the photocatalytic performance of ZnO/ZnSe heterojunction.

To estimate the photocatalytic capacity of ZnO/ZnSe heterostructure, methyl orange was selected as the target pollutant. Figure 5 demonstrates the UV–visible absorption spectrum of degraded methyl orange solution. As depicted in Fig. 5, the maximum peak at 460 nm gradually decreased under the irradiation of Xe lamp. In addition, blank experiments without the photocatalyst and similar experiments using bare ZnO rods and spherical ZnSe samples were carried out to rationalize the photocatalytic ability of ZnO/ZnSe heterostructure. With the prolongation of the reaction time, the absorption peaks of three samples decreased gradually, and methyl orange degraded gradually with time. Compared with ZnO rod (Fig. 5a) and spherical ZnSe (Fig. 5b), the heterostructure of ZnO/ZnSe exhibited stronger photocatalytic activity, which was caused by the slight larger active surface and effective separation of electron–holes of heterostructure (Fig. 5c).

The photocatalytic degradation curves of methyl orange in ZnO, ZnSe and ZnO/ZnSe samples irradiated by Xe lamp were shown in Fig. 5d, where C_0 was the initial concentration of methyl orange, while C was the concentration in the reaction process after equilibrium adsorption. On the contrary, the degradation rate of ZnO/ZnSe after 9 h was about 94.3%, while that of ZnO rod and ZnSe sample was about 24% and 68%, respectively. Obviously, the highest degradation rate of ZnO/ZnSe sample could be explained by improved the charge transport capacity. On one hand, the slightly exposed active surface of ZnSe was sensitive to the process of promoting surface carrier transfer. The specific surface areas of ZnO, ZnSe and ZnO/ZnSe were calculated by BET method with 7.477, 38.776 and 7.561 m^2/g, respectively (See Supplementary Fig. S2). The results showed that ZnO/ZnSe heterostructure was beneficial to slightly increased the specific surface area compared with that of ZnO.[24,25] On the other hand, the absorption capacity and effective electron–hole separation could be enhanced due to the coupling effect between ZnO and ZnSe, and the improved electron transport ability could greatly inhibit the recombination probability of charge carriers in ZnO/ZnSe, thus greatly improving their photocatalytic reactions.[25,26]

The mechanism of photocatalytic degradation could be understood on the basis of energy level alignment, as shown in Fig. 6. When light irradiated on the surface of ZnO/ZnSe, electrons would be excited to the conduction band, leaving holes in the ZnSe valence band. Then, under the action of diffusion potential energy caused by the ZnO/ZnSe heterostructure type II band alignment, electrons migrated to the ZnO conduction band. In this way, the electrons and holes were well separated, thus reducing the probability of electron-hole pair recombination. The holes in the ZnSe valence band could

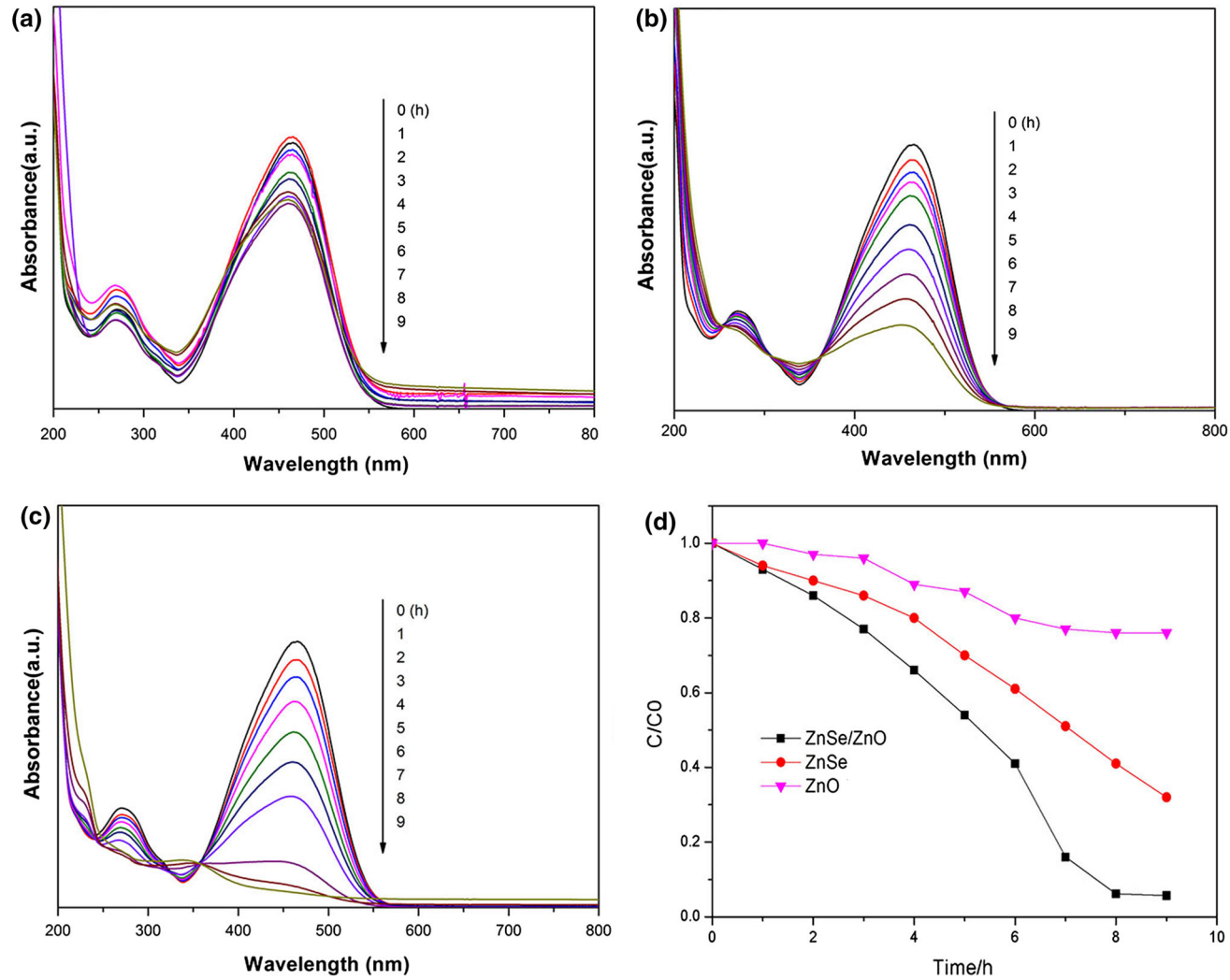

Fig. 5. Relationship between light irradiation time and photocatalytic degradation of methyl orange (a) ZnO, (b) ZnSe, (c) ZnO/ZnSe, and (d) photocatalytic degradation rates of ZnO, ZnSe and ZnO/ZnSe samples irradiated by Xe lamp.

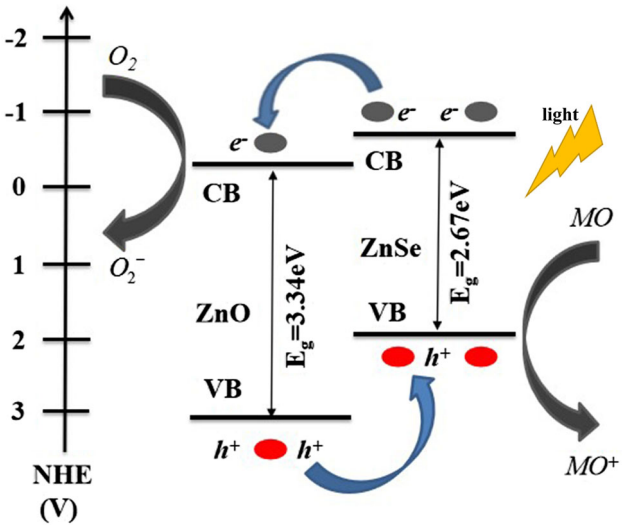

Fig. 6. Energy level alignment of ZnO/ZnSe heterostructure.

directly oxidize organic dye molecules, and the electrons in the ZnO conduction band would react with O_2 to form superoxide radical anions.

CONCLUSIONS

Here, we presented a structure of spherical ZnSe particles grown on ZnO rods. The ZnO/ZnSe heterostructure was fabricated by simple combination of ultrasonic and hydrothermal synthetic methods. The ammonia provided an alkaline environment for se^{2-}, with the increase of OH^-, more $Zn(OH)_4^{2-}$ were formed by ZnO and further reacted with Se^{2-} to obtain the heterostructure of ZnO/ZnSe. It was believed that the ammonia concentration was an improtant factor determining the nucleation and growth rate of ZnO/ZnSe heterostructure. The relationship between structure and photocatalytic activity was also studied. The ZnO/ZnSe heterostructure exhibited excellent photocatalytic performance for the degradation of

methyl orange, which was caused by the enhancement of light absorption and effective charge transport property of spherical ZnSe, which were caused by the coupling of ZnO and ZnSe. This work may also provides a simple way to design functional semiconductors with appropriate band gaps and high photocatalytic activity.

ACKNOWLEDGMENTS

This work was supported by National Natural Science Foundation of China (No. 51406069); China Postdoctoral Science Foundation Special Project (No. 2016T90426); China Postdoctoral Science Foundation (No. 2015M581733); Jiangsu Planned Projects for Postdoctoral Research Funds (No. 1501107B); Training Project of Jiangsu University Youth Backbone Teacher.

CONFLICT OF INTEREST

The authors declare that they have no conflict of interest.

ETHICAL APPROVAL

This article does not contain any studies with human participants or animals performed by any of the authors.

AVAILABILITY OF DATA

The data sets supporting the results of this article are included within the article and its additional files.

ELECTRONIC SUPPLEMENTARY MATERIAL

The online version of this article (https://doi.org/10.1007/s11664-019-07209-3) contains supplementary material, which is available to authorized users.

REFERENCES

1. K.M. Lee, C.W. Lai, K.S. Ngai, and J.C. Juan, *Water Res.* 88, 428 (2016).
2. W. Yu, J. Zhang, and T. Peng, *Appl. Catal. B Environ.* 181, 220 (2016).
3. F. Achouri, S. Corbel, L. Balan, K. Mozet, E. Girot, G. Medjahdi, M. Said, A. Ghrabi, and R. Schneider, *Mater. Des.* 101, 309 (2016).
4. Z.C. Wu, H. Wang, Y.J. Xue, B. Li, and B.Y. Geng, *J. Mater. Chem. A* 2, 17502 (2014).
5. C. Kulsi, A. Ghosh, A. Mondal, K. Kargupta, S. Ganguly, and D. Banerjee, *Appl. Surf. Sci.* 392, 540 (2017).
6. M. Mitra, A. Ghosh, A. Mondal, K. Kargupta, S. Ganguly, and D. Banerjee, *Appl. Surf. Sci.* 402, 418 (2017).
7. F. Qiao, Q.C. Liang, X.J. Cui, Q. Xu, Y. Xie, and H. Chu, *Energy Environ.* 135, 12608 (2018). https://doi.org/10.30919/esee8c187.
8. F. Qiao, Q. Liang, J. Yang, Z. Chen, and Q. Xu, *J. Electron. Mater.* 48, 2338 (2019). https://doi.org/10.1007/s11664-019-06988-z.
9. C. Kulsi, A. Ghosh, A. Mondal, K. Kargupta, S. Ganguly, and D. Banerjee, *Mater. Res. Express.* 4, 035902 (2017).
10. X. Gu, C. Li, S. Yuan, M. Ma, Y. Qiang, and J. Zhu, *Nanotechnology* 27, 402001 (2016).
11. Y. Liu, S. Wei, and W. Gao, *J. Hazard. Mater.* 287, 59 (2015).
12. H. Liu, Y. Hu, Z. Zhang, X. Liu, H. Jia, and B. Xu, *Appl. Surf. Sci.* 355, 644 (2015).
13. G. Chen, X. Song, H. Zhang, X. Zhang, J. Zhang, Y. Wang, J. Gao, Y. Zhao, C. Zhang, and J. Tao, *Surf. Coat. Technol.* 320, 467 (2017).
14. S. Rasal, P.V. More, C. Hiragond, S. Jadhav, and P.K. Khanna, *Adv. Mater.* 7, 390 (2016).
15. M. Ding, N. Yao, C. Wang, J. Huang, M. Shao, S. Zhang, P. Li, X. Deng, and X. Xu, *Nanoscale Res. Lett.* 11, 205 (2016).
16. Y. Yang, H. Li, F. Hou, J. Hu, X. Zhang, and Y. Wang, *Mater. Lett.* 180, 97 (2016).
17. Y. Liu, C. Xu, Z. Zhu, J. Lu, A.G. Manohari, and Z. Shi, *Res. Bull.* 98, 64 (2018).
18. G.R.S. Andrade, C.C. Nascimento, Z.M. Lima, E.T. Neto, L.P. Costa, and I.F. Gimenez, *Appl. Surf. Sci.* 399, 573 (2017).
19. K.S. Ngai, W.T. Tan, Z. Zainal, R.M. Zawawi, and J.C. Juan, *Sci. Adv. Mater.* 8, 788 (2016).
20. H. Chu, W. Han, F. Ren, L. Xiang, Y. Wei, and C. Zhang, *ES Energy Environ.* 2, 73 (2018).
21. H. Chu, W. Han, W. Cao, M. Gu, and G. Xu, *Energy* 166, 392 (2019).
22. C. Coll, D. Notter, F. Gottschalk, T. Sun, C. Som, and B. Nowack, *Nanotoxicology* 10, 436 (2016).
23. Y. Zhao, J. Ma, L. Liu, and Y. Bao, *Colloid Surf. A* 518, 57 (2017).
24. M. Laurent, S. Stassi, G. Canavese, and V. Cauda, *Adv. Mater. Interfaces* 4, 16007581 (2017).
25. V.M. Nguyen, W. Li, V.H. Pham, L. Wang, P. Sheng, Q. Cai, and C. Grimes, *J. Colloid Interfaces Sci.* 462, 389 (2016).
26. L. Wang, G. Tian, Y. Chen, Y. Xiao, and H. Fu, *Nanoscale* 8, 9366 (2016).